21

Induced Perturbations and Adopted Conformations in Membranes by the HIV-1 Fusion Peptide

José L. Nieva, Nerea Huarte, Shlomo Nir, and David P. Weliky

Abstract

The human immunodeficiency virus type 1 (HIV-1) fusion peptide spans a sequence of ca. 25 amino acid residues located at the N terminus of the spike transmembrane subunit gp41. This hydrophobic and conserved domain is required for the induction of the cell–virus membrane fusion event that initiates the replication cycle. HIV-1 fusion peptide–membrane interactions have been studied using synthetic derivatives and model membranes. This chapter focuses on the description of two interrelated aspects of this approach: (1) membrane destabilization (function) detected as permeabilization or fusion of vesicles, or both, with defined lipid composition, and (2) adopted conformation (structure) by the peptide associated with the same model membranes.

21

Induced Perturbations and Adopted Conformations in Membranes by the HIV-1 Fusion Peptide

José L. Nieva,[1] Nerea Huarte,[1] Shlomo Nir,[2] and David P. Weliky[3]

[1]Biophysics Unit (CSIC-UPV/EHU) and University of the Basque Country, Bilbao, Spain*
[2]Seagram Center for Soil and Water Sciences, School of Agricultural, Food and Environmental Quality Sciences, The Hebrew University of Jerusalem, Rehovot, Israel
[3]Department of Chemistry, Michigan State University, East Lansing, Michigan, USA

21.1. Introduction

Fusion between cell and viral membranes constitutes a key step of the human immunodeficiency virus (HIV) infectious cycle. This process, activated upon specific surface receptor engagement by the envelope

*Universidad del País Vasco, Bilbao, España (Euskal Herriko Unibertsitatea, Bilbo, Espainia).

protein (Env), promotes the translocation of the capsid into the $CD4^+$ host-cell interior where virus replication takes place.[1,2] To this end, the fusogenic gp41 transmembrane Env subunit makes use of a collapsible ectodomain structure (the hairpin or six-helix bundle) that opens and closes and a non-constitutive membrane anchor, the fusion peptide (FP) that ensures coupling of hairpin closure to apposition and fusion of cell and viral membranes.[3]

HIV-1 FP (HFP) spans a conserved, hydrophobic amino acid sequence of about 25 residues located at the free N terminus of gp41.[4] It is assumed that it becomes exposed in the vicinity of the target membrane and has the intrinsic capacity of inserting therein. It is also postulated that the interaction of this hydrophobic stretch with the bare target membrane would be sufficient to induce destabilization leading to fusion. In principle, this latter process would depend solely on the capacity of the peptide to bind the membrane lipidic components.

To gain insights into the functional implication of this sequence in the HIV fusion process, HFP–membrane interactions have been characterized by several groups using representative synthetic peptides and model membranes. Nieva and co-workers employed large unilamellar vesicles (LUVs), made either of 1-palmitoyl-2-oleoylphosphatidylglycerol (POPG) or an equimolar mixture of dioleoylphosphatidylcholine (DOPC)–dioleoylphosphatidylethanolamine (DOPE)–cholesterol (Chol), in an attempt to model the acidic and the neutral lipid fraction, respectively, of the invaded cell plasma membrane.[5–7] Further improvements by Weliky's group included the use of LM3 vesicles containing 1-palmitoyl-2-oleoylphosphatidylcholine (POPC), 1-palmitoyl-2-oleoylphosphatidylethanolamine (POPE), 1-palmitoyl-2-oleoylphosphatidylserine (POPS), sphingomyelin, phosphatidylinositol, and cholesterol in a 10:5:2:2:1:10 mol ratio, a mixture that approximates more closely the lipid composition of HIV-1 host cell membranes.[8–10]

From these studies it can be concluded that HFP may exist in bilayers, adopting different main conformations depending on conditions such as the peptide-to-lipid mol ratio, the membrane lipid composition (specifically the presence of Chol), or the concentration of divalent cations. This conformational polymorphism might be of physiological relevance. On one hand, it might contribute to the flexibility of the fusogenic complex during the fusion reaction cycle if, as suggested by the hairpin model,[1,2] the rod-shaped gp41 ectodomain alternates between conformations perpendicular and parallel to the target bilayer normal. On the other,

conformational switching might be related to the HFP capacity of inducing membrane perturbations, a phenomenon that might underlie its active role in the HIV-1–cell fusion process.

21.2. FP-Induced Membrane Perturbations: Leakage and Fusion

This section describes the bilayer destabilization processes induced by HFP. Two different conditions have been selected to illustrate dissimilar effects: (1) lytic pore formation in dispersed POPG vesicles (**Figs. 21.1** and **21.2**), and (2) aggregation and fusion of DOPC–DOPE–Chol (1:1:1 molar ratio) vesicles (**Fig. 21.3**).

These studies were based on the use of a synthetic HFP representing a 23 amino acid sequence at the conserved N terminus of HIV-1 gp41 (LAV_{1a} strain), which was initially denoted as HIV_{arg} (sequence AVGIGALFLGFLGAAGSTMGARS). HIV_{arg} was synthesized in C-terminal carboxamide form by solid-phase methods and 9-fluorenylmethoxycarbonyl (Fmoc) chemistry protocols. Trifluoroacetic acid (TFA) acidolysis followed by reverse-phase high-performance liquid chromatography (HPLC) purification produced homogeneous (>95% content in the target sequence by HPLC) materials with the expected molecular mass. The purified peptide was dissolved in dimethylsulfoxide (dimethyl sulfoxide (DMSO), spectroscopy grade) and its concentration was determined by the bicinchoninic-acid microassay (Pierce, Rockford, IL, USA). Small, diluted aliquots (typically 20 μL, 1 mg/mL) were stored frozen and were thawed only once, upon use.

LUVs were prepared according to the extrusion method.[11] Phospholipids and cholesterol, purchased from Avanti Polar Lipids (Birmingham, Ala., USA) and Sigma (St. Louis, Mo., USA), respectively, were mixed in chloroform and dried under a N_2 stream. Traces of organic solvent were removed by overnight vacuum pumping. Subsequently, dried lipid films were dispersed in buffer and subjected to 10 freeze-thaw cycles before extruding them 10 times through two stacked polycarbonate membranes (Nuclepore, Inc., Pleasanton, Calif., USA). Vesicle size distributions were determined by using a laser particle size NICOMP 370 (Santa

Barbara, Calif., USA). Extrusion through membranes of nominal pore size 0.1μm produces POPG and DOPC–DOPE–Chol vesicles with mean diameters (± standard deviation, SD) of 95 ± 28 and 124 ± 38 nm, respectively (**Figs. 21.2** and **21.3**). When solutes were encapsulated in the liposomes, internal and external osmolarities were adjusted by adding NaCl. The osmolarities of all solutions were routinely measured in a cryoscopic osmometer (Osmomat 030, Gonotec, Berlin, Germany). Lipid concentrations of liposome suspensions were determined by phosphate analysis.

21.2.1. Leakage and Pore Formation in POPG Vesicles

The lytic pore model[12,13] presupposes that HFP binds and becomes rapidly incorporated into the bilayer, while once within the membranes, peptide aggregation occurs. When an aggregate within a membrane has reached a critical size, a channel or transmembrane pore is created within the membrane, and leakage of encapsulated molecules can occur. Thus, it is assumed that discrete peptide structures within isolated vesicles are responsible for the observed membrane permeabilization, as opposed to the general destabilization of the bilayer architecture that is observed when negatively charged vesicles are aggregated by divalent cations.

Cryo-transmission electron microscopy (cryo-TEM) indeed revealed that HFP-induced permeabilization operated within isolated vesicles (**Fig. 21.1A**). In fair agreement with the dynamic light scattering determinations of vesicle size distribution, cryo-TEM micrographs of POPG vesicles extruded through membranes of nominal pore size 0.1μm showed a homogeneous population of dispersed spherical particles with diameters in the range of 100 nm (**Fig. 21.1A**, left panel). Treatment of these vesicles with HFP under conditions inducing the total release of their aqueous content (see below) did not appreciably alter their overall morphology (right panel). Dynamic light scattering further confirmed a mean diameter value (±SD) of 110 ± 19 nm for the vesicles treated with peptide. Additional biochemical evidence supported that lytic structures formed by HFP are long-lived and exist in dispersed POPG LUVs.[14] Thus, vesicles totally permeabilized by pre-addition of HFP sustained entry of solutes into their aqueous internal space. The peptide also induced efficient leakage from POPG LUVs doped with distearoylphosphatidylethanolamine-poly(ethylene glycol) (MW of poly(ethylene

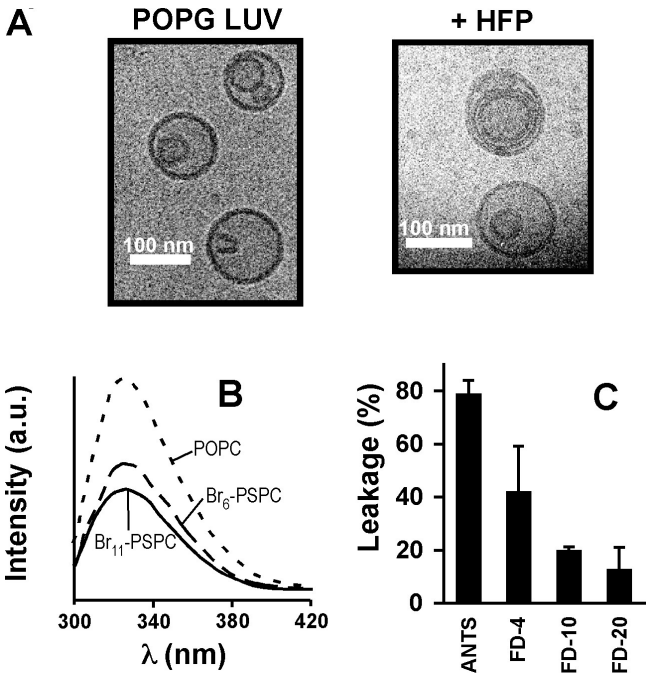

Figure 21.1. HFP interaction with POPG vesicles. (**A**) Cryo-TEM micrographs of extruded LUV without peptide (**left**) and treated with HFP at a peptide-to-lipid mole ratio of 1:70 (**right**). (**B**) Fluorescence emission spectra of the F8W analog incubated with POPG–POPC, POPG–Br_6-PSPC and POPG–Br_{11}-PSPC vesicles (2:1 mole ratio). Vesicle concentration was 0.1 mM and the peptide-to-lipid mole ratio 1:200. (**C**) HFP-induced leakage of solutes of different sizes encapsulated into POPG vesicles. Final extents were obtained after incubating peptide and vesicles for 10 min at a peptide-to-lipid molar ratio of 1:100. Means ± SD of four independent experiments are presented.

glycol) ca. 2000). These vesicles did not aggregate even at the highest tested HFP concentrations.

In the canonical pore structure,[12,13] individual peptides are proposed to have a predominantly α-helical secondary structure and the helix axis is aligned perpendicularly to the bilayer surface. The proposed extent of helical structure of HFP in the POPG bilayer received direct support from infrared (IR) spectroscopy measurements (see **Section 21.3** below).[5,14] Deep penetration of the peptide into the bilayer core could be inferred from the Trp fluorescence quenching by the hydrophobic matrix-residing brominated phospholipids, according to the method described by Bolen

and Holloway (**Fig. 21.1B**).[15] These experiments were carried out using the F8W peptide, a derivative in which Trp conservatively substituted for the HFP Phe8 residue, and POPG vesicles containing 1-palmitoyl-2-oleoyl-phosphatidylcholine (POPC) or the brominated phospholipids 1-palmitoyl-2-stearoyl(6,7)dibromo-*sn*-glycero-3-phosphocholine (Br_6-PSPC) or 1-palmitoyl-2-stearoyl(11,12)dibromo-*sn*-glycero-3-phosphocholine (Br_{11}-PSPC) (Avanti Polar Lipids, Birmingham, Ala., USA). The integral areas of the spectra displayed in **Fig. 21.2B** denoted that Br_{11}-PSPC quenched F8W-Trp more efficiently than Br_6-PSPC (estimated quenching percentages of 51% and 41%, respectively). Bromine atoms quench by a short-range process that requires a close approach to the fluorophore.[15] This would be consistent with the Trp residue being located closer to the C_{11}–C_{12} than to the C_6–C_7 position within the acyl chain region of the bilayer.

The size of a transbilayer pore as that proposed by the model also dictates the upper bound on the size (and shape) of molecules that can leak. Assembly of size-limited HFP pores was confirmed by comparing the leakage of encapsulated solutes of different MWs (**Fig. 21.1C**). Permeabilization to low-molecular-weight markers was monitored by the ANTS–DPX assay,[16,17] which is based on the quenching of 8-aminonaphthalene-1,3,6-trisulfonic acid disodium salt (ANTS, MW 427) fluorescence by *p*-xylene bis(pyridinium)bromide (DPX, MW 422) (Molecular Probes, Junction City, Oreg., USA). ANTS and DPX are true markers of the aqueous space of the liposomes, and when co-encapsulated, DPX efficiently quenches ANTS fluorescence by collisional transfer. In addition, both ANTS and DPX remain trapped for extended periods. When both probes are released to the medium, dilution of DPX prevents quenching of ANTS fluorescence outside the liposomes. POPG LUVs containing 12.5mM ANTS, 45mM DPX, 20 mM NaCl, and 5mM 4-(2-hydroxyethyl)-1-piperazineethanesulfonic acid (HEPES) were obtained by separating the unencapsulated probes by gel filtration in a Sephadex G-75 column eluted with 5 mM HEPES, 100 mM NaCl (pH 7.4). Fluorescence measurements were performed by setting the ANTS emission at 520 nm and the excitation at 355 nm. A cutoff filter (470 nm) was placed between the sample and the emission monochromator to avoid directly scattered light from liposomes.

Fluorescein isothiocyanate (FITC) dextrans with average MWs 4400 (FD-4), 9500 (FD-10), and 19600 (FD-20) (obtained from Sigma,

St. Louis, Mo., USA) were used for assessing permeabilization to high-MW markers.[18] These probes were encapsulated in POPG LUVs at the self-quenching concentration of 75 mg/mL in 5 mM HEPES, 40 mM NaCl at pH 7.4. Non-entrapped material was removed in this case by gel filtration on a Sephacryl S-300 high-resolution column eluted with 5 mM HEPES, 65 mM NaCl, pH 7.4. Solute release was monitored as dequenching of FITC fluorescence following the dilution of vesicle contents into the medium. Fluorescein dequenching was monitored by setting the excitation at 465 nm and the emission at 530 nm. A cutoff filter at 495 nm was used in emission. The data displayed in **Fig. 21.1C** show that under conditions allowing efficient HFP-induced ANTS leakage from POPG LUVs, FD-4 was partly retained in the aqueous lumen of the liposomes, while FD-10 and FD-20 were not significantly released into the medium. This would be consistent with a maximal size of the HFP pore.

A mathematical model was then employed for the analysis of HFP-induced ANTS–DPX leakage. This model was previously described in detail.[5,12,13] The computational procedure in the case of HFP peptide included several refinements (see **Fig. 21.2A**). The analysis proceeded in two stages. First, the minimal number of peptides required to form a pore, M, was determined from a fit of the final extent of leakage (**Fig. 21.2B**). This step required an estimation of the binding constant, K, of peptides to vesicles of a given size. According to the model, the final extent of leakage is due to the leakage of contents from all the vesicles containing M or more peptides, where M is the critical number of peptides in the aggregate.

For a completely homogeneous population of vesicles, the final extent of leakage $L \equiv L(\infty)$ is given by

$$L = \sum_{i=M}^{N} A_i/G_0 \qquad \textbf{(21.1)}$$

in which N is the largest number of peptides that can bind to a single vesicle, G_0 is the molar concentration of vesicles, and A_i is the concentration of vesicles containing i incorporated peptides. The dimensionless quantities $\overline{A}_i = A_i/G_0$ represent the distribution function, satisfying the relation

$$\sum_{i=0}^{N} A_i/G_0 = \sum_{i=0}^{N} \overline{A}_i = 1 \qquad \textbf{(21.2)}$$

The procedure for calculating the functions A_i was previously described by Nir and co-workers.[12] A refinement in the HFIP procedure included a determination of the distribution of vesicle sizes as already described. This information is crucial in any attempt to employ simulations and predictions for the final extent and kinetics of leakage, since the encapsulated volume depends on the third power of the internal radius. The modified expression of **Eq. 21.1** is

$$L = \sum_{j=1}^{m} \sum_{i=M}^{N} \overline{A}_{ij} f_j \qquad \textbf{(21.3)}$$

in which f_j is the fraction of encapsulated volume in vesicles of size j. A value of $m = 10$ was used for the number of vesicle sizes considered **(Fig. 21.2A)**. It has to be noted that, for each size, the value of the binding constant, K, was separately calculated by the program, assuming that the intrinsic affinity for peptide binding was independent of vesicle size. The results were essentially independent of the value of N used in the calculations, provided it was sufficiently large. $N = 2000$ was used for the vesicles of the largest size.

After determining the value of M, the number of peptides required for pore formation, the forward rate of peptide aggregation, C (units of s^{-1}) could be determined. The relevant parameter in the calculation of the kinetics of leakage is the dimensionless quantity $\tau = Cit$, where t is the time (s) and i is proportional to the surface concentration of the peptides (units = 1/area). For the same value of i, the number of peptides per vesicle, the surface density is larger for the smaller vesicles. This was taken into account by the program. A value of C that corresponds to the outer surface area of a 100 nm radius vesicle was reported. The same values of M and C were used for all peptide-to-lipid ratios.

Fig. 21.2B illustrates the dependence of the extent of leakage on the peptide-to-lipid ratios. At a 1:25 ratio leakage was complete, whereas at a 1:750 ratio only 3.3% leakage was observed at equilibrium. Calculations were performed to simulate the experimental values and determine M, the minimal number of peptides required to form a pore. Such calculations generated the normalized distribution of vesicles containing i peptides (see **Eqs. 21.1** and **21.2**) from knowledge of the binding constant, K. A range of K values or binding ratios was assumed and for each value the calculated values of final extents and kinetics of leakage were generated. In these

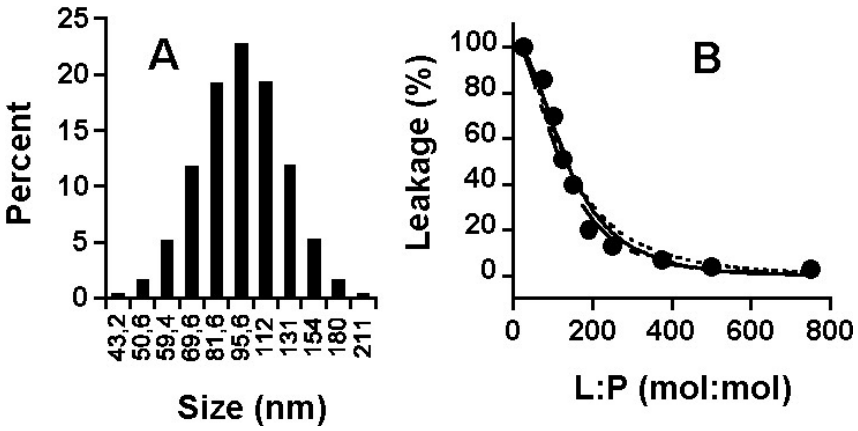

Figure 21.2. Pore formation in POPG vesicles. (**A**) Vesicle-size distribution used in the mathematical model calculation. (**B**) Extents of ANTS leakage experimentally obtained (circles) and simulations for *M* values of 4, 6, and 10, dotted, slashed, and continuous lines, respectively. The best fit to the experimental values was obtained for $M = 6$.

calculations the peptide-to-lipid ratios varied from 1:25 to 1:750. The range of *M* values that could yield a simulation of the final extents and kinetics of leakage varied from $M = 4$ to $M = 10$. Outside this range some of the deviations between calculated and experimental values doubled. The experimental values of final extent of leakage could be simulated fairly well by using $M = 6$ (**Fig. 21.2B**).

21.2.2. Induction of Fusion of Cholesterol-Containing Liposomes

The interaction of the HFP peptide with DOPC–DOPE–Chol vesicles resulted in the adoption of an extended structure restricted to the outer membrane monolayer. This version of the peptide was by itself sufficient to aggregate vesicles and perturb lipid packing, thereby inducing the type of bilayer destabilization required for membrane merger. This interaction pattern could be initially inferred from the analysis of the vesicle morphology by cryo-TEM.[19,20] Suspensions of vitrified DOPC–DOPE–Chol LUVs showed a mean diameter in the range of 100 nm (**Fig. 21.3A**, left panel). A majority of vesicles displayed a stomatocyte-like morphology, which suggested the existence of an initial invaginated state. In

samples treated with the peptide, large aggregates could be discerned consisting of fusion products that contained highly curved structures (**Fig. 21.3A**, upper right panel). These samples also displayed isolated vesicles whose morphology consisted of membrane protrusions and beaded tubes (**Fig. 21.3A**, bottom right panel). The existence of membrane protrusions would be consistent with a differential increase in the area of the vesicle external monolayer, caused by an insertion of the externally added peptide restricted to this leaflet of the surface-constrained bilayer (i.e., vesicle bilayers).

A peptide location close to the lipid–water interface was suggested by the next set of experiments. The bilayer level to which the peptide penetrated was again assessed by the bromolipid assay (**Fig. 21.3B**).[15] To perform the measurements in this case, either Br_6-PSPC or Br_{11}-PSPC was used instead of DOPC in target vesicles. Both Br_6-PSPC and Br_{11}-PSPC quenched Trp fluorescence to some extent, but the former showed a higher quenching efficiency. Thus as opposed to POPG (**Fig. 21.2B**), Trp8 in DOPC–DOPE–Chol bilayers was located closer to the C_6–C_7 than to the C_{11}–C_{12} acyl-chain position. This is consistent with insertion within an acyl chain region closer to the interface than to the hydrocarbon core center.

HFP-promoted fusion was assessed using a membrane lipid mixing assay described by Struck et al. (**Fig. 21.3C**).[21] The assay is based on the resonance energy transfer (RET) from the fluorescent probe N-(7-nitrobenz-2-oxa-1,3-diazol-4-yl)phosphatidylethanolamine (N-NBD-PE) to N-(lissamine Rhodamine B sulfonyl)phosphatidylethanolamine (N-Rh-PE) (Avanti Polar Lipids, Birmingham, Ala., USA). RET occurs when both lipid probes are near each other as components of the same bilayer. Dilution due to membrane mixing with unlabeled vesicles results in RET decrease and concomitant increase in NBD-PE fluorescence. Vesicles containing 0.6 mol % of each probe were mixed with unlabeled vesicles at 1:1 ratio. The NBD emission was monitored at 530 nm with the excitation wavelength set at 465 nm. A cutoff filter at 515 nm was used between the sample and the emission monochromator to significantly reduce scattering interferences. The fluorescence scale was calibrated such that the zero level corresponded to the initial residual fluorescence of the labeled vesicles and the 100% level to complete mixing of all the lipids in the system. The latter value was set by the fluorescence intensity of vesicles, labeled with 0.3 mol % each of the fluorophores, at the same total lipid

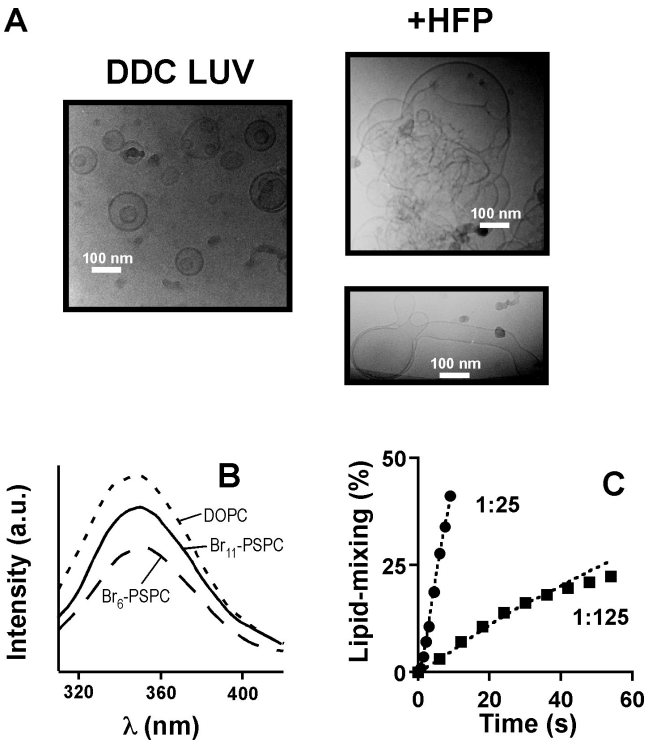

Figure 21.3. HFP interaction with DOPC–DOPE–Chol vesicles. (**A**) Cryo-TEM micrographs of control untreated and peptide-containing (added peptide-to-lipid mole ratio 1:10) LUV samples (**left** and **right panels**, respectively). Vesicle–vesicle fusion products and membrane protrusions are shown in **right top** and **bottom** panels, respectively. (**B**) Fluorescence emission spectra of F8W analog incubated with DOPC–DOPE–Chol, Br_6-PSPC–DOPE–Chol, and Br_{11}-PSPC–DOPE–Chol vesicles. (**C**) Kinetics of HFP-induced membrane–lipid mixing measured at 1:25 and 1:125 peptide-to-lipid molar ratios. Experimental results are given by the curves, the data points represent values obtained from simulation of the results using a mass-action kinetic model.

concentration as that in the fusion assay. It should be noted that, in the concentration range of the fluorophores used, the NBD-PE fluorescence intensity increases linearly with the dilution of the probes.[21]

To further characterize the fusogenicity of HFP, the rate constants of peptide-induced vesicle fusion were calculated.[7] Only the changes in this kinetic parameter allowed determining the HFP involvement in the fusion reaction itself as opposed to possible effects at the level of the preceding

Table 21.1. Rate constants of HIV_{arg}-induced aggregation and fusion of DOPC–DOPE–Chol LUVs

Peptide-to-Lipid Mole Ratio	Rate Constant of Fusion, f (s^{-1})	Rate Constant of Aggregation, C (M^{-1} s^{-1})	Rate Constant of Dissociation, D (s^{-1})
1:25	0.2	10^9	0.001
1:100	0.03	8×10^8	0.001
1:125	0.02	7×10^8	0.001

aggregation step. The analysis of the kinetics of fusion of DOPC–DOPE–Chol LUVs considered aggregation, dissociation, and fusion processes and involved the determination of the rate constants of those processes, namely, aggregation C ($M^{-1.}s^{-1}$), dissociation D (s^{-1}), and fusion f (s^{-1}). The calculations were performed by introducing certain modifications into the program as described by Nir et al.[22]

Table 21.1 illustrates that the fusion rate constant increased by number: 10-fold, from 0.02 s^{-1} to 0.2 s^{-1}, when the peptide-to-lipid ratio increased from 1:125 to 1:25. This indicates that the HFP was directly involved in the fusion process, which supports the notion that HFP is necessary and sufficient for destabilizing two interacting membranes to induce fusion.

21.3. Structural Characterization by Low-Resolution Techniques

The intrinsic flexible nature of the HFP sequence is reflected by the circular dichroism (CD) spectra obtained in different environments (**Fig. 21.4**). The soluble FPK3 derivative, which incorporated three Lys at its C terminus, displayed in solution CD spectra with prominent negative peaks around 200 nm (dotted line), characteristic of species with no predominant secondary structure. In the presence of dodecylphosphocholine (DPC) micelles (continuous lines), the spectrum showed a positive band centered at 190 nm and negative bands at ca. 208 and 222 nm,

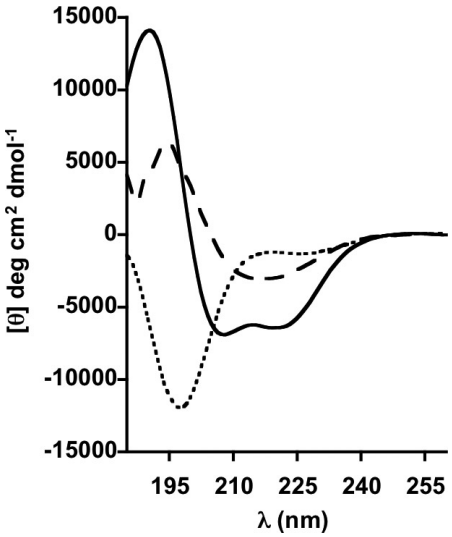

Figure 21.4. Structural plasticity of HFP. CD spectra of the peptide were obtained in buffer (dotted line), buffer containing 5 mM DPC (continuous line) and co-dispersed with 1 mM POPC–Chol–Phosphatidic acid (2:1:0.2 mole ratio) vesicles (slashed line). Peptide concentration in the samples was 30 μM.

characteristic of sequences with a high α-helix content. Yet a different main secondary structure was observed when the peptide was codispersed with Chol-containing vesicles (dashed lines). In these samples the positive peak shifted toward higher wavelengths, and negative absorption was centered at 217 nm, indicating the presence of β-sheet-like extended structures.

IR spectroscopy allowed the determination of the membrane-bound HFP secondary structure, under conditions that closely reproduced leakage and fusion experiments.[5,6,14] Thus, in an attempt to approximate those conditions, before IR measurements, samples were processed as follows (see also **Fig. 21.5**). Peptide dissolved in DMSO was added to a stirred solution of lipid vesicles prepared in D_2O buffer, so that the desired lipid-to-peptide molar ratio was reached in diluted samples. After at least 30 min incubation at room temperature, centrifugation of the peptide-lipid complexes gave rise to a homogeneous band of vesicles floating on top of the D_2O. In the case of DOPC–DOPE–Chol LUVs, electron micrographs of the floating fraction in control samples (CTL)

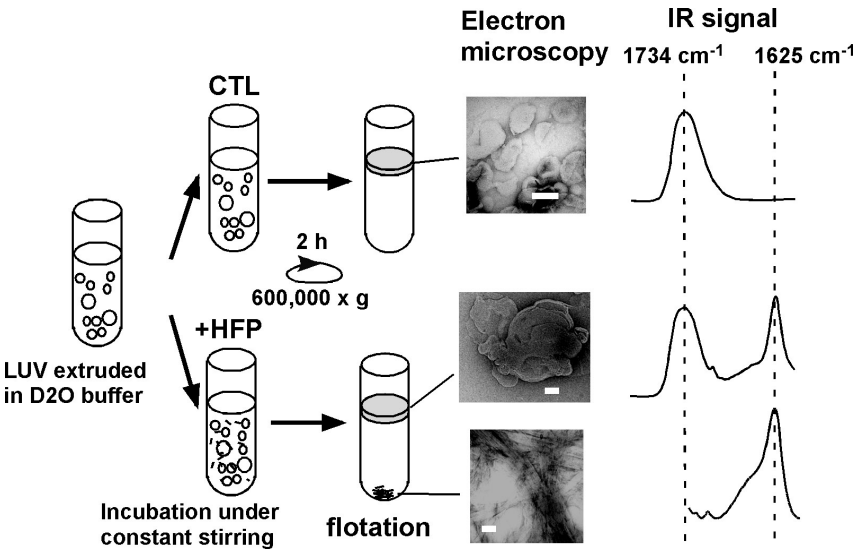

Figure 21.5. Flotation method for preparing vesicle–peptide IR samples. See text for the explanation (scale bars = 100 nm).

without peptide showed vesicles of a size in the range of 100 nm (**Fig. 21.5**). In contrast, the floating fraction of samples treated with the peptide (+HFP) revealed larger structures of vesicle–vesicle fusion products. Micrographs of the unbound peptide in the precipitates consisted of fibrillar bundles, which could not be observed floating with vesicles. Hence, the peptides associated with floating-fused vesicles were not discernible by electron microscopy.

Samples obtained from the concentrated floating fractions were collected and subsequently placed between two CaF_2 windows separated by 50 μm spacers. IR spectra were recorded in a Nicolet 520 spectrometer equipped with a DTGS **(**deuterated triglycine sulfate) detector. 200 scans of sample and 200 scans of reference were taken for each spectrum, using a shuttle device. Solvent contribution was eliminated by subtracting the pure buffer spectrum from the original one. The criterion used was to maintain a straight baseline between 1300 and 1900 cm^{-1} with the maximum difference factor not giving rise to negative lobes. The spectra were then transferred to a personal computer where standard Fourier self-deconvolution and Fourier derivation methods were used.[23]

The IR spectrum of floating vesicles devoid of peptide displayed an intense band centered at 1734 cm^{-1}, which corresponds to the C=O stretching vibration of the phospholipid ester bonds.[23] In addition to this phospholipid band, DOPC–DOPE–Chol membranes treated with the HFP displayed an intense absorption maximum at 1625 cm^{-1} and a less intense maximum at 1689 cm^{-1} within the conformation-sensitive amide I region. The latter signal was also observed in the precipitate samples and came from peptides adopting a β-like extended conformation.[23]

IR studies of the peptide-lipid complexes floating in D_2O buffer indicated the existence of different HFP conformations in DOPC–DOPE–Chol and POPG vesicles (**Fig. 21.6**). The peptide, in DOPC–DOPE–Chol samples, adopted the same predominant extended structure at the various peptide-to-lipid ratios tested. In contrast, when bound to negatively charged POPG vesicles the conformation-sensitive amide I region of the peptide displayed a main band centered at 1652 cm^{-1}, indicating a preferential α-helical conformation. In this latter case, the α helix is predominant at membrane doses allowing efficient permeation of solutes through HFP pores. A signal consistent with the accumulation of extended structures could be observed in this system only at high peptide loads, for example, 1:10 peptide-to-lipid mole ratio.

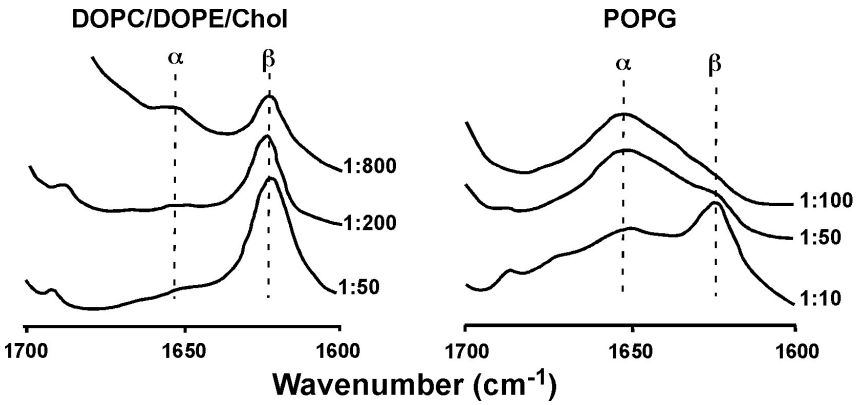

Figure 21.6. Structural characterization by IR. The conformation-sensitive amide I region of the IR spectrum is shown for vesicle–peptide complexes collected from floating fractions (**Figure 21.5**). DOPC–DOPE–Chol (**left**) or POPG (**right**) vesicles were treated with peptide at the indicated doses prior to flotation.

In summary, IR studies of membrane-bound HFP demonstrate the existence of conformational polymorphism in the sense that depending on the vesicle composition the peptide may adopt different secondary structures. Moreover, these different HFP structures can be associated with the induction of dissimilar membrane perturbations. The type of perturbation induced by the extended structure compromises the overall bilayer organization, allowing intermembrane mixing of constituent lipids. HFP adopting a helical conformation, on the other hand, establishes discrete structures (pores) through which solutes can cross the membrane in both directions.

21.4. Characterization by High-Resolution NMR Techniques

21.4.1. Background and Sample Preparation

NMR spectroscopy has provided significant information about the structure of HFP, and the studies can generally be divided into liquid-state NMR spectroscopy of HFP in detergent micelles and solid-state NMR spectroscopy of HFP in membranes. To date, the liquid-state NMR studies have provided more complete structures, while the solid-state NMR studies are probably more biologically relevant. The reason for this assertion is that HFP does not induce fusion between detergent micelles but does induce fusion between membrane vesicles.[6,8]

Preparation of NMR samples in detergent micelles is straightforward and is typically dissolution of lyophilized peptide in a detergent solution. There are more variants to the solid-state NMR preparation, but they can generally be divided into two approaches. The first method is cosolubilization of dry HFP and lipid in organic solvent followed by removal of the solvent and then hydration. The second method is mixing of an aqueous solution of HFP with an aqueous solution containing LUVs followed by centrifugation to pellet the LUVs with associated bound HFP. NMR spectra are then acquired for the pellets. This second approach has greater functional relevance because HFP incorporation in membranes is similar to that of leakage, lipid-mixing, and content-mixing assays.

However, this approach also relies on being able to separate membrane-associated and nonmembrane-associated HFP; that is, nonmembrane-associated HFP should not pellet. As displayed in **Fig. 21.5**, HFP tends to aggregate in aqueous solution and there has therefore been considerable effort to create conditions under which HFP aggregation is minimized. In one approach HFP was made with nonnative lysines on the C terminus and aggregation was inhibited by electrostatic repulsion of the positively charged lysine side-chains at neutral pH.[24] In a second approach, pelleting of HFP by centrifugation was examined in solutions containing different buffers and salts, and it was observed that pelleting was minimized in organic buffers such as HEPES and that pelleting was maximal in phosphate buffer and in buffers containing NaCl.[8] Analytical ultracentrifugation data demonstrated monomeric peptide in a solution containing 0.1 mM lysine-tagged HFP and 5 mM HEPES buffer at pH 7.0.[10,24] These are suitable conditions for solid-state NMR sample preparation. In addition, very similar NMR spectra were obtained for membrane incorporation of HFP under these conditions and with the organic co-solubilization approach.[24] This similarity suggested that both approaches yielded the thermodynamic equilibrium rather than kinetically trapped structure.

21.4.2. HFP in Detergent Micelles

Several groups have done liquid-state NMR in micelles, and there is general agreement that for peptide-to-detergent ratios ≤ 0.02 the contiguous residues between Ile-4 and Leu-12 are helical.[25–29] There is some disagreement about the helical extent of the more C-terminal residues, and there are reports of (1) a straight helix from Ile-4 to Met-19 with some helical character extending to residue 22; (2) a helix-turn-helix motif with the first helix between Ile-4 and Gly-16; and (3) a straight helix from Ile-4 to Ala-14 and disordered conformation beyond Ala-14. Although there is general agreement that Ala-15 is close to the micelle interface, there is also some disagreement about the extent to which the apolar N-terminal region of HFP traverses the micelle or is on the micelle surface.[25] In one study, there were two sets of chemical shifts observed for residues Gly-5 to Leu-12, and both sets were consistent with helical conformation.[29] One interpretation of these data was that each set corresponded to a distinct micelle location of this apolar region. For peptide-to-detergent ratios ≈ 0.1, the NMR line widths were broad and

correlated with peptide aggregation. Sharp lines could be recovered with addition of detergent and suggested that the aggregation is reversible. Aggregation was consistent with observation of β conformation in the CD spectrum of HFP in detergent at peptide-to-detergent ratio of 0.1.[30]

21.4.3. HFP Conformation in Membranes

The structure of HFP in membranes as probed by solid-state NMR is more complex than the HFP structure in detergent micelles. The solid-state NMR measurements can be divided generally into measurements of conformation and tertiary structure, measurements of HFP location in membranes, and measurements of the orientation of an HFP helix relative to the membrane bilayer normal. The ^{13}C chemical shifts, intramolecular ^{13}CO–^{15}N distance measurements (CO ≡ carbonyl), and slow-spinning two-dimensional exchange experiments have been useful probes of conformation. **Table 21.2** summarizes some of the experimental data and includes distributions of ^{13}CO chemical shifts for different conformations derived from chemical-shift databases.[8,10,31–34] The peak shift and standard deviation (in parentheses) of each distribution are listed. In membranes without cholesterol, there is a significant fraction of helical conformation, at least between residues Leu-7 and Phe-11. In line with the previously

Table 21.2. Experimental solid-state NMR data for membrane-associated HFP

Residue	Expt. Chem Shifts in ppm		Chem. Shift Distributions in ppm		Other expt. data in membrances	Expt. Dihedral Angles in Membranes w/Chol	
	Membranes w/o Chol	Membranes with Chol	Helix	β-strand	Without Chol	ϕ	ψ
Val-2		174.5	177.7(1.4)	174.8(1.4)		−160°	140°
Ala-6		173.7	179.4(1.3)	176.1(1.5)	Leu-7 ^{13}CO··· Phe-11 ^{15}N distance = 4.1 ± 0.1 Å		
Leu-7	178.8	173.4	178.5(1.3)	175.7(1.5)			
Phe-8	178.4	172.9	177.1(1.4)	174.3(1.6)		−120°	115°
Leu-9		173.9	178.5(1.3)	175.7(1.5)		−130°	130°
Gly-10		170.7	175.5(1.2)	172.6(1.6)			
Phe-11		172.6	177.1(1.4)	174.3(1.6)		−165°	140°

described IR results (**Fig. 21.3**), for membranes with cholesterol, there is predominant β-strand conformation for residues between Val-2 and Ala-14. The membranes of host cells of HIV contain ~30 mol % cholesterol, which suggests that the β conformation may have biological relevance.[35,36] The NMR signals of Ala-1 and of the residues' C terminal of Ala-14 were relatively broad, which indicated greater conformational disorder.

21.4.4. HFP Tertiary Structure

There is not yet information about possible oligomerization of HFP in its helical conformation. There have been studies about the tertiary structure and oligomerization of the β conformation. In particular, there have been measurements of the distance proximity of labeled backbone ^{13}CO nuclei to labeled ^{15}N nuclei in membrane-associated HFP. The labeling and sample preparation were done to ensure that intramolecular ^{13}CO–^{15}N distances were long compared to intermolecular ^{13}CO–^{15}N distances. There have been two important results from these studies: (1) There is proximity (less than 6 Å) of ^{13}CO nuclei on one strand with ^{15}N nuclei on an adjacent strand.[9] Although IR, electron spin resonance, and fluorescence resonance energy transfer (FRET) studies have implied a significant population of hydrogen-bonded β-strand oligomers, the solid-state NMR distance measurements have provided more definitive evidence for these oligomers.[30] (2) There appear to be a population of parallel β strands that are approximately in-register and a population of antiparallel strands with adjacent strand crossing near Phe-8 and Leu-9.[9,32,37] For both arrangements, most of the apolar N-terminal 16 residues would have interpeptide hydrogen bonds, which is consistent with residues being predominantly located in the apolar membrane interior where there is little water available for hydrogen bonding.

21.4.5. Membrane Location of HFP

A reasonable hypothesis is that HFP-induced membrane perturbation is related to HFP membrane location and correlates with fusion catalysis. Solid-state NMR has provided some pertinent information about membrane location through measurements of the distance proximities of labeled ^{13}CO nuclei in the HFP backbone to ^{31}P nuclei in the lipid head groups. One important result is that the Ala-14 to Gly-16 residues are

closer to the ^{31}P nuclei than are the residues between Gly-5 and Gly-13.[38] In addition, the Ala-1 to Gly-3 residues are close to ^{31}P nuclei. These were the results both for cholesterol-containing membranes and for membranes without cholesterol, and they suggest that the membrane location of HFP is approximately the same for the respective helical and strand conformations. In addition, the location of the Ala-1 to Gly-3 and the Ala-14 to Gly-16 residues near the membrane–water interface correlates with liquid-state NMR data that these residues are near the micelle–water interface for the helical conformation of HFP.[25,27] These residues are at the termini of the apolar region of the HFP, and a reasonable membrane or micelle location model would have the intervening residues located toward the membrane or micelle interior. It is striking that the membrane location appears generally independent of conformation, and this idea may be related to the observation that significant HFP-induced lipid mixing is observed between vesicles that lack cholesterol and vesicles that contain cholesterol.[10] As described earlier in the chapter, these membrane compositions correspond to significant helical and predominant β-strand conformations, respectively. A reasonable hypothesis is therefore that membrane location rather than conformation is a significant determinant of HFP fusion activity.

21.4.6. Membrane Insertion Angle of HFP

A general hypothesis in the fusion peptide literature is that membrane perturbation and fusion activity are correlated with partial insertion of a fusion peptide helix into the membrane interior and that the insertion is "tilted," that is, the angle between the helix axis and the membrane normal is 30° to 70°.[39] An initial study to determine this angle with solid-state NMR was unsuccessful most likely because the high peptide-to-lipid ratio resulted in a significant fraction of β conformation.[40] A more recent study suggested a relatively small angle between the helix axis and the membrane normal.[41]

21.4.7. Correlation of Structural Results with Fusion Activity

The most straightforward model for the fusogenic structure of HFP is a single conformation. Arguments in favor of a fusogenic helical

conformation include that fact that (1) other membrane-perturbing peptides are helical and (2) membrane perturbation would likely be induced by tilted partial insertion. Arguments in favor of the β-strand conformation include the fact that (1) both fusion activity and β-strand conformation are favored at higher peptide-to-lipid ratios and (2) this conformation is predominant in cholesterol-containing membranes that mimic the membranes of host cells of HIV. In fact, comparable HFP fusion activity has been detected using vesicles with or without cholesterol and correlates with helical or β-strand conformation, respectively.[10] An argument has therefore been made that the fusogenic conformation is transient and does not have regular secondary structure.[42,43] Evidence supporting this argument includes the nonsystematic effect on fusion activity of substitution of D amino acids for L amino acids in the HFP. As detailed earlier, membrane location is another structural parameter likely related to fusion activity and the data to date suggest that at least the Ala-1 to Gly-3 and the Ala-14 to Ala-16 residues have similar locations in both membranes and in micelles and in helical and strand conformations. Similar membrane locations are then an alternative hypothesis for the similar fusion activities of helical and β-strand HFP. It is also noted that high-resolution X-ray structures exist for fusion proteins of class II enveloped viruses.[44] There are internal rather than N-terminal fusion peptides in these viruses and the fusion peptides have predominantly extended but not β-sheet structure.

21.4.8. Future Studies

NMR has contributed substantially to the development of high-resolution structural models for HFP in detergent micelles and in membranes. Future studies may better define the location of helical HFP in micelles as well as the extent of helical structure in micelles and membranes. There are good correlations between the mutation-fusion activity relationships in HFP and in HIV, and comparative NMR studies of mutants may therefore provide insight into the structural basis for HFP fusion activity.[6] NMR may also be applied to characterize constructs that contain HFP and that have greater biological relevance. In particular, (1) longer N-terminal regions of gp41 that include HFP have been made, and (2) cross-linked HFPs with three HFP strands have been synthesized to mimic the expected HFP topology in trimeric gp41.[10,32,37,45–48] These

more biologically relevant constructs had much greater fusion activity than did the ~25-residue HFP. NMR structural studies on these constructs will be possible if sufficient (1–5 mg) quantities can be straightforwardly prepared. There are good prospects for such preparations as evidenced by recent work on a construct for the full influenza fusion protein ectodomain including the fusion peptide.[49] Sufficient quantities of the influenza protein were made so that ^{13}C chemical shifts were measured at specific residues in the membrane-associated protein, and the residue conformations determined from the shifts.

References

1. Doms RW and Moore JP. **HIV-1 membrane fusion: Targets of opportunity.** *J Cell Biol* 2000, **151**:F9–14.
2. Gallo SA, Finnegan CM, Viard M, Raviv Y, Dimitrov A, Rawat SS, Puri A, Durell S, and Blumenthal R. **The HIV Env-mediated fusion reaction.** *Biochim Biophys Acta* 2003, **1614**:36–50.
3. Melikyan GB, Markosyan RM, Hemmati H, Delmedico MK, Lambert DM, and Cohen FS. **Evidence that the transition of HIV-1 gp41 into a six-helix bundle, not the bundle configuration, induces membrane fusion.** *J Cell Biol* 2000, **151**: 413–423.
4. Nieva JL and Agirre A. **Are fusion peptides a good model to study viral cell fusion?** *Biochim Biophys Acta* 2003, **1614**:104–115.
5. Nieva JL, Nir S, Muga A, Goni FM, and Wilschut J. **Interaction of the HIV-1 fusion peptide with phospholipid vesicles: Different structural requirements for fusion and leakage.** *Biochemistry* 1994, **33**:3201–3209.
6. Pereira FB, Goni FM, Muga A, and Nieva JL. **Permeabilization and fusion of uncharged lipid vesicles induced by the HIV-1 fusion peptide adopting an extended conformation: Dose and sequence effects.** *Biophys J* 1997, **73**:1977–1986.
7. Nieva JL, Nir S, and Wilschut J. **Destabilization and fusion of zwitterionic large unilamellar lipid vesicles induced by a b-type structure of the HIV-1 fusion peptide.** *J Liposome Res* 1998, **8**:165–182.
8. Yang J, Gabrys CM, and Weliky DP. **Solid-state nuclear magnetic resonance evidence for an extended beta strand conformation of the membrane-bound HIV-1 fusion peptide.** *Biochemistry* 2001, **40**:8126–8137.

9. Yang J and Weliky DP. **Solid state nuclear magnetic resonance evidence for parallel and antiparallel strand arrangements in the membrane-associated HIV-1 fusion peptide.** *Biochemistry* 2003, **42**:11879–11890.

10. Yang R, Prorok M, Castellino FJ, and Weliky DP. **A trimeric HIV-1 fusion peptide construct which does not self-associate in aqueous solution and which has 15-fold higher membrane fusion rate.** *J Am Chem Soc* 2004, **126**:14722–14723

11. Hope MJ, Bally MB, Webb G, and Cullis PR. **Production of large unilamellar vesicles by a rapid extrusion procedure. Characterization of size distribution, trapped volume and ability to maintain a membrane potential.** *Biochim Biophys Acta* 1985, **812**:55–65.

12. Parente RA, Nir S, and Szoka FC Jr. **Mechanism of leakage of phospholipid vesicle contents induced by the peptide GALA.** *Biochemistry* 1990, **29**:8720–8728.

13. Nir S and Nieva JL. **Interactions of peptides with liposomes: Pore formation and fusion.** *Prog Lipid Res* 2000, **39**:181–206.

14. Saez-Cirion A and Nieva JL. **Conformational transitions of membrane-bound HIV-1 fusion peptide.** *Biochim Biophys Acta* 2002, **1564**:57–65.

15. Bolen EJ and Holloway PW. **Quenching of tryptophan fluorescence by brominated phospholipid.** *Biochemistry* 1990, **29**:9638–9643.

16. Ellens H, Bentz J, and Szoka FC. **pH-induced destabilization of phosphatidylethanolamine-containing liposomes: Role of bilayer contact.** *Biochemistry* 1984, **23**:1532–1538.

17. Ellens H, Bentz J, and Szoka FC. **H+- and Ca2+-induced fusion and destabilization of liposomes.** *Biochemistry* 1985, **24**:3099–3106.

18. Basanez G, Zhang J, Chau BN, Maksaev GI, Frolov VA, Brandt TA, Burch J, Hardwick JM, and Zimmerberg J. **Pro-apoptotic cleavage products of Bcl-xL form cytochrome c-conducting pores in pure lipid membranes.** *J Biol Chem* 2001, **276**:31083–31091.

19. Pereira FB, Valpuesta JM, Basanez G, Goni FM, and Nieva JL. **Interbilayer lipid mixing induced by the human immunodeficiency virus type-1 fusion peptide on large unilamellar vesicles: The nature of the nonlamellar intermediates.** *Chem Phys Lipids* 1999, **103**:11–20.

20. Agirre A, Flach C, Goni FM, Mendelsohn R, Valpuesta JM, Wu F, and Nieva JL. **Interactions of the HIV-1 fusion peptide with large unilamellar vesicles and monolayers. A cryo-TEM and spectroscopic study.** *Biochim Biophys Acta* 2000, **1467**:153–164.

21. Struck DK, Hoekstra D, and Pagano RE. **Use of resonance energy transfer to monitor membrane fusion.** *Biochemistry* 1981, **20**:4093–4099.

22. Nir S, Stegmann T, and Wilschut J. **Fusion of influenza virus with cardiolipin liposomes at low pH: Mass action analysis of kinetics and extent.** *Biochemistry* 1986, **25**:257–266.

23. Arrondo JL, Muga A, Castresana J, and Goni FM. **Quantitative studies of the structure of proteins in solution by Fourier-transform infrared spectroscopy.** *Prog Biophys Mol Biol* 1993, **59**:23–56.

24. Yang J, Prorok M, Castellino FJ, and Weliky DP. **Oligomeric beta-structure of the membrane-bound HIV-1 fusion peptide formed from soluble monomers.** *Biophys J* 2004, **87**:1951–1963.

25. Chang DK, Cheng SF, and Chien WJ. **The amino-terminal fusion domain peptide of human immunodeficiency virus type 1 gp41 inserts into the sodium dodecyl sulfate micelle primarily as a helix with a conserved glycine at the micelle-water interface.** *J Virol* 1997, **71**:6593–6602.

26. Morris KF, Gao XF, and Wong TC. **The interactions of the HIV gp41 fusion peptides with zwitterionic membrane mimics determined by NMR spectroscopy.** *Biochim Biophys Acta-Biomembr* 2004, **1667**:67–81.

27. Jaroniec CP, Kaufman JD, Stahl SJ, Viard M, Blumenthal R, Wingfield PT, and Bax A. **Structure and dynamics of micelle-associated human immunodeficiency virus gp41 fusion domain.** *Biochemistry* 2005, **44**:16167–16180.

28. Li YL and Tamm LK. **Structure and plasticity of the human immunodeficiency virus gp41 fusion domain in lipid micelles and bilayers.** *Biophys J* 2007, **93**:876–885.

29. Gabrys CM and Weliky DP. **Chemical shift assignment and structural plasticity of a HIV fusion peptide derivative in dodecylphosphocholine micelles.** *Biochim Biophys Acta-Biomembr* 2007, **1768**:3225–3234.

30. Gordon LM, Curtain CC, Zhong YC, Kirkpatrick A, Mobley PW, and Waring AJ. **The amino-terminal peptide of HIV-1 glycoprotein 41 interacts with human erythrocyte membranes: Peptide conformation, orientation and aggregation.** *Biochim Biophys Acta* 1992, **1139**:257–274.

31. Bodner ML, Gabrys CM, Parkanzky PD, Yang J, Duskin CA, and Weliky DP. **Temperature dependence and resonance assignment of ^{13}C NMR spectra of selectively and uniformly labeled fusion peptides associated with membranes.** *Magn Reson Chem* 2004, **42**:187–194.

32. Zheng Z, Qiang W, and Weliky DP. **Investigation of finite-pulse radiofrequency-driven recoupling methods for measurement of intercarbonyl distances in polycrystalline and membrane-associated HIV fusion peptide samples** *Magn Reson Chem* 2007, **245**:S247–S260.

33. Bodner ML, Gabrys CM, Struppe JO, and Weliky DP. **^{13}C-^{13}C and ^{15}N-^{13}C correlation spectroscopy of membrane-associated and uniformly labeled human**

immunodeficiency virus and influenza virus fusion peptides: Amino acid-type assignments and evidence for multiple conformations. *J Chem Phys* 2008, **128**(5):052319.

34. Zhang HY, Neal S, and Wishart DS. **RefDB: A database of uniformly referenced protein chemical shifts.** *J Biomol NMR* 2003, **25**:173–195.

35. Aloia RC, Tian H, and Jensen FC. **Lipid composition and fluidity of the human immunodeficiency virus envelope and host cell plasma membranes.** *Proc Natl Acad Sci U S A* 1993, **90**:5181–5185.

36. Brugger B, Glass B, Haberkant P, Leibrecht I, Wieland FT, and Krasslich HG. **The HIV lipidome: A raft with an unusual composition.** *Proc Natl Acad Sci U S A* 2006, **103**:2641–2646.

37. Zheng Z, Yang R, Bodner ML, and Weliky DP. **Conformational flexibility and strand arrangements of the membrane-associated HIV fusion peptide trimer probed by solid-state NMR spectroscopy.** *Biochemistry* 2006, **45**:12960–12975.

38. Qiang W, Yang J, and Weliky DP. **Solid-state nuclear magnetic resonance measurements of HIV fusion peptide to lipid distances reveal the intimate contact of β strand peptide with membranes and the proximity of the Ala-14-Gly-16 region with lipid headgroups.** *Biochemistry* 2007, **46**:4997–5008.

39. Peuvot J, Schanck A, Lins L, and Brasseur R. **Are the fusion processes involved in birth, life and death of the cell depending on tilted insertion of peptides into membranes?** *J Theor Biol* 1999, **198**:173–181.

40. Curtain C, Separovic F, Nielsen K, Craik D, Zhong Y, and Kirkpatrick A. **The interactions of the N-terminal fusogenic peptide of HIV-1 gp41 with neutral phospholipids.** *Eur Biophys J* 1999, **28**:427–436.

41. Wasniewski CM, Parkanzky PD, Bodner ML, and Weliky DP. **Solid-state nuclear magnetic resonance studies of HIV and influenza fusion peptide orientations in membrane bilayers using stacked glass plate samples.** *Chem Phys Lipids* 2004, **132**:89–100.

42. Hofmann MW, Weise K, Ollesch J, Agrawal P, Stalz H, Stelzer W, Hulsbergen F, de Groot H, Gerwert K, Reed J, and Langosch D. **De novo design of conformationally flexible transmembrane peptides driving membrane fusion.** *Proc Natl Acad Sci U S A* 2004, **101**:14776–14781.

43. Reichert J, Grasnick D, Afonin S, Buerck J, Wadhwani P, and Ulrich AS. **A critical evaluation of the conformational requirements of fusogenic peptides in membranes.** *Eur Biophys J* 2007, **36**:405–413.

44. Gibbons DL, Vaney MC, Roussel A, Vigouroux A, Reilly B, Lepault J, Kielian M, and Rey FA. **Conformational change and protein protein interactions of the fusion protein of Semliki Forest virus.** *Nature* 2004, **427**:320–325.

45. Tan K, Liu J, Wang J, Shen S, and Lu M. **Atomic structure of a thermostable subdomain of HIV-1 gp41.** *Proc Natl Acad Sci U S A* 1997, **94**:12303–12308.

46. Caffrey M, Cai M, Kaufman J, Stahl SJ, Wingfield PT, Covell DG, Gronenborn AM, and Clore GM. **Three-dimensional solution structure of the 44 kDa ectodomain of SIV gp41.** *EMBO J* 1998, **17**:4572–4584.

47. Sackett K and Shai Y. **The HIV-1 gp41 N-terminal heptad repeat plays an essential role in membrane fusion.** *Biochemistry* 2002, **41**:4678–4685.

48. Yang R, Yang J, and Weliky DP. **Synthesis, enhanced fusogenicity, and solid state NMR measurements of cross-linked HIV-1 fusion peptides.** *Biochemistry* 2003, **42**:3527–3535.

49. Curtis-Fisk J, Preston C, Zheng Z, Worden RM, and Weliky DP. **Solid-state NMR structural measurements on the membrane-associated influenza fusion protein ectodomain.** *J Am Chem Soc* 2007, **129**:11320–11321.